Review

Probing Magnetic Fields in Young Supernova Remnants with IXPE

Patrick Slane [1,*], Riccardo Ferrazzoli [2], Ping Zhou [3] and Jacco Vink [4]

1   Center for Astrophysics, Harvard & Smithsonian, 60 Garden Street, Cambridge, MA 02138, USA
2   INAF Istituto di Astrofisica e Planetologia Spaziali, Via del Fosso del Cavaliere 100, 00133 Roma, Italy; riccardo.ferrazzoli@inaf.it
3   School of Astronomy and Space Science, Nanjing University, Nanjing 210023, China; pingzhou@nju.edu.cn
4   Anton Pannekoek Institute for Astronomy & GRAPPA, University of Amsterdam, Science Park 904, 1098 XH Amsterdam, The Netherlands; j.vink@uva.nl
*   Correspondence: slane@cfa.harvard.edu

Abstract: Synchrotron emission from the shocked regions in supernova remnants provides, through its polarization, crucial details about the magnetic field strength and orientation in these regions. This, in turn, provides information on particle acceleration in these shocks. Due to the rapid losses of the highest-energy relativistic electrons, X-ray polarization measurements allow for investigations of the magnetic field to be carried outvery close to the sites of particle acceleration. Measurements of both the geometry of the field and the levels of turbulence implied by the observed polarization degree thus provide unique insights into the conditions leading to efficient particle acceleration in fast shocks. The Imaging X-ray Polarimetry Explorer (IXPE) has carried out observations of multiple young SNRs, including Cas A, Tycho, SN 1006, and RX J1713.7−3946. In each, significant X-ray polarization detections provide measurements of magnetic field properties that show some common behavior but also considerable differences between these SNRs. Here, we provide a summary of results from IXPE studies of young SNRs, providing comparisons between the observed polarization and the physical properties of the remnants and their environments.

Keywords: X-rays; polarimetry; supernova remnants; cosmic ray; particle acceleration; magnetic field turbulence; individual objects: Cas A, Tycho's SNR, SN 1006, RX J1713.7−3946

1. Introduction

Over the past two decades, it has become clear that the rapid shocks in young supernova remnants (SNRs) are capable of accelerating particles to extremely high energies. Particle acceleration most likely proceeds through diffusive shock acceleration (DSA), wherein energetic particles streaming away from the shock scatter off of magnetohydrodynamical waves—either pre-existing in the ambient plasma or generated by other streaming ions—and return to the shock for additional acceleration, e.g., [1]. This process builds up a nonthermal population of high-energy particles, with the maximum energy being limited by radiative losses, the age of the SNR, or particle escape [2]. Such particle acceleration by SNR shocks has long been suggested as a process by which Galactic cosmic rays are produced, up to energies approaching the "knee" of the cosmic ray spectrum at $\sim 10^{14}$–10^{15} eV.

The details of this acceleration process are very much still under investigation. The standard picture for DSA requires strong magnetic fields and high levels of turbulence in order for the efficient return of particles to the acceleration site. Particle transport is generally described in terms of a mean-free path that is a factor η times the particle gyroradius. The maximum acceleration efficiency for the loss-limited case that applies to electrons in young SNRs (because of high synchrotron losses) is obtained for $\eta = 1$,

the so-called Bohm limit for which the mean-free path is the minimum value. The associated photon cutoff energy for synchrotron emission from electrons in this process is $\epsilon_0 \approx 1.6\eta^{-1}(v_{\rm sh}/4000 \text{ km s}^{-1})^2$ keV [3]. To produce photons up to several keV, high shock speeds are required, such as those found in very young SNRs. In addition, small Bohm factors are required, indicating highly turbulent magnetic fields.

The above description holds in the so-called "test particle" limit where the energy of the accelerated particles is dynamically unimportant. If the relativistic particle component of the energy density becomes comparable to that of the thermal component, the shock acceleration process can become highly nonlinear. The gas becomes more compressible, which results in higher magnetic fields and enhanced acceleration.

For most of the known young SNRs, thin rims of nonthermal X-ray emission surround the remnants directly along their forward shocks. These observations make it clear that SNRs are capable of accelerating electrons to very high energies. The observed rim widths are typically 3–5 arcsec—resolvable only with *Chandra*—and lead to field strengths ranging from ∼100 to 500 μG, demonstrating significant amplification of the typical 3 μG upstream field in the interstellar medium.

The nature of the turbulence that plays such a crucial role in the acceleration process is not yet fully understood. The cosmic ray current associated with the highest-energy particles, which escape the acceleration region, produces turbulence in the upstream region [4]. This is ultimately swept up by the shock, where the component of the field that is tangent to the shock front is compressed. This leads to an expectation of synchrotron radiation with a radial polarization (i.e., with the electric vector oriented along the radial direction). Such polarization is indeed observed in radio observations of older SNRs [5,6] (see the latter reference for a recent review). However, radio observations of young SNRs like Cas A, Tycho, and others show tangential polarization, indicating radial magnetic fields in the downstream region [5]. The nature of these radial fields is not well understood. Particle-in-cell simulations indicate that the acceleration process is more efficient for shocks whose velocity vectors are parallel to the magnetic field. One suggestion for the observed parallel fields in young remnants is simply that one observes radiation from regions where the acceleration is most efficient [7]. Alternatively, density fluctuations—possibly in the form of clumps from material upstream—can form magneto-driven instabilities in the downstream region that drive radial magnetic fields [8], suggesting that the ambient medium into which the SNRs expand might play a significant role. Recent studies indicate that the Bell instability can produce density fluctuations sufficient to drive this same mechanism without any requirement for a pre-existing clumpy environment [9].

In any such mechanism, the question of magnetic field orientation and the amplitude of the associated turbulence are fundamentally important. Both of these parameters can be probed with polarization. Because of the short synchrotron lifetimes of X-ray-emitting electrons, X-ray polarization explores the magnetic orientation and turbulence very close to the particle acceleration site, and thus represents a particularly important tool for constraining the acceleration process.

In its first two years, the IXPE has observed six SNRs. Here, we summarize results of the initial four studies, with observations of Cassiopeia A, Tycho's SNR, the northeast limb of SN 1006, and the northwest region of RX J1713.7−3946. We present a general introduction of the properties of each remnant, summarize the IXPE observations and results for each, and then discuss the results in the context of models for polarization in SNRs.

2. Cas A

Cas A is the relic of a core-collapse supernova estimated to have occurred roughly 350 years ago. Located at a distance of 3.4 kpc [10], it is one of the brightest SNRs in the radio and X-ray bands. Expansion measurements establish a forward shock velocity of ∼5000 km s^{-1}, e.g., [11,12]. Radio polarization measurements establish a polarization

degree (PD) of ∼5% in the bright ejecta-rich shell and 8–10% in the outer regions near the forward shock [13]. The polarization angle (PA) implies a radial magnetic field [14,15].

X-ray observations with *BeppoSAX* and RXTE revealed the presence of synchrotron emission from particles with energies up to ∼10 TeV [16,17], consistent with the acceleration of particles by the rapid shocks. *Chandra* observations establish that the nonthermal X-rays arise from thin regions [18,19] whose 1″–2″ widths imply magnetic field strengths of 250–500 μG, e.g., [20,21], implying significant magnetic field amplification.

The IXPE observed Cas A in 2022 for ∼900 ks [22]. A pixel-by-pixel search revealed modest evidence for X-ray polarization with polarization degrees of 5–15%, and with indications of radial magnetic fields. By assuming circular symmetry of the polarization direction, however, larger emission regions could be combined to improve sensitivity. These measurements established highly significant detections of polarization from multiple regions, including the forward shock and reverse shock, and marginal evidence for similar polarization from a distinct region on the western edge of the reverse shock, illustrated in Figure 1 (left), where we present a three-band color IXPE image of Cas A with these regions identified. Figure 1 (right) shows the polarization results for the entire SNR, where the polarization degree is represented by the radial component of the polar plot and the polarization angle is measured relative to the radial direction. Contours show confidence intervals, and the pink circle illustrates the minimum detectable polarization at 99% confidence for this observation. Significant polarization is detected from the forward shock and reverse shock (RS) regions, along with the entire SNR. The PA values for all regions are consistent with tangential polarization—and thus radial magnetic fields—with PD values ranging from ∼2 to 4%. Using *Chandra* spectra for the individual regions to determine fluxes for both the nonthermal emission and the (unpolarized) thermal emission, the corrected PD values for the X-ray synchrotron radiation range from ∼2 to 5%—lower than observed in the radio band.
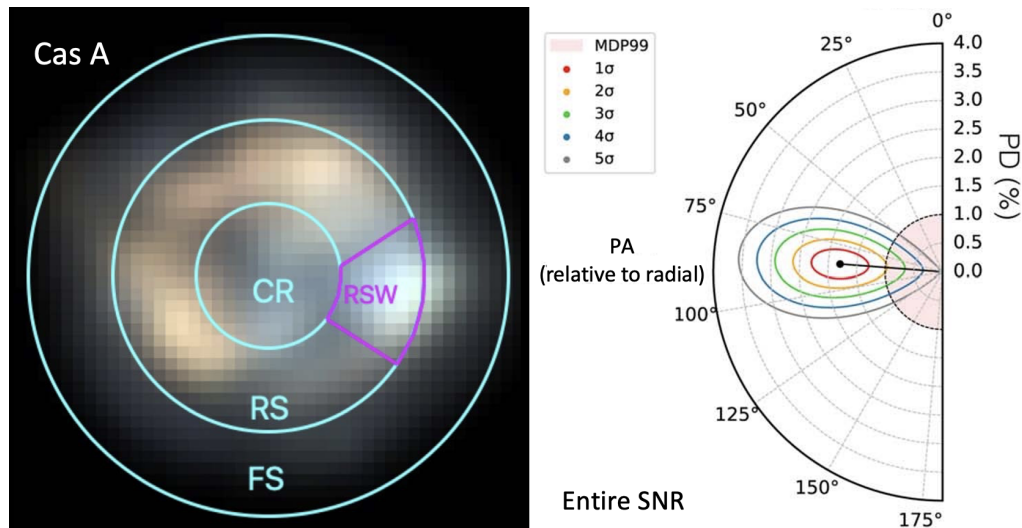
Figure 1. **Left**: IXPE image of Cas A. Labels identify the central region (CR), reverse shock (RS), western reverse shock (RSW), and forward shock (FS) investigated in [22]. **Right**: Polar plot for emission from entire SNR. The polarization degree is indicated on the radial axis and the polarization angle is shown, with 0° corresponding to the radial direction; an angle of 90° indicates a radial magnetic field direction. The contours show significance levels.

The low polarization degree measured with the IXPE implies high levels of turbulence in the region close to the shock, implying that despite the shock compression that should produce a primarily tangential field at the shock, magnetic fields are reoriented on spatial scales corresponding to the thin rims ($\sim 10^{17}$ cm).

3. Tycho's SNR

Tycho's SNR is the remnant of the historical supernova SN 1572 [23]. Unlike Cas A, a core-collapse remnant, Tycho is the result of a Type Ia explosion. Its shock velocity is in the range of 3500–4400 km s^{-1} [24,25]. Radio emission from Tycho at 2.8–6 cm is polarized, with typical polarization degree values ranging from 0 at the center to 7–8% at the outer rim, with the direction of the polarization indicating a large-scale radial magnetic field structure [26–30]. High-resolution Chandra X-ray observations of Tycho revealed a bright thin synchrotron rim at the shock [31] matching similar features seen in the radio band [28], but also peculiar small-scale structures (from ∼arcseconds to ∼arcminute) in the 4–6 keV band—the so-called "stripes" in the western rim that were first identified by [32]. These small-scale structures are variable in time and shape on a scale of a few years [33,34]. The stripes, along with the entire SNR rim, are thought to be CR acceleration sites, and might be the result of fast energy losses of the TeV electrons emitting X-rays downstream of the shock in amplified magnetic fields [35]. If that is the case, the synchrotron structures are due to geometric projection of the thin regions where the TeV electrons are accelerated; the expectations of their polarization properties were extensively discussed prior to the IXPE launch [35–37].

The IXPE observed Tycho during 2022, for a total exposure time of ∼990 ks [38]. The analysis followed a strategy similar to the one used for Cas A, starting with a pixel-by-pixel search of the signal. However, since Tycho is not as bright as Cas A, the polarization map binned on a 1-arcminute scale does not show highly significant detections.

By aligning and summing up the data from different regions of interest shown in Figure 2, such as the highest significance region in the west (region f), the rim (region g), and also the whole remnant, highly significant detections of polarized emission were identified. The measured tangential direction of polarization corresponds to a radial magnetic field, consistent with the radio band polarization observations but originating from regions even closer to the shock. The degree of X-ray polarization in Tycho is significantly higher than that for Cas A: in Tycho, the synchrotron PD was found to be $12 \pm 2\%$ in the rim and $9 \pm 2\%$ in the whole remnant. These results are compatible with the expectation of turbulence produced by an anisotropic cascade of a radial magnetic field near the shock.
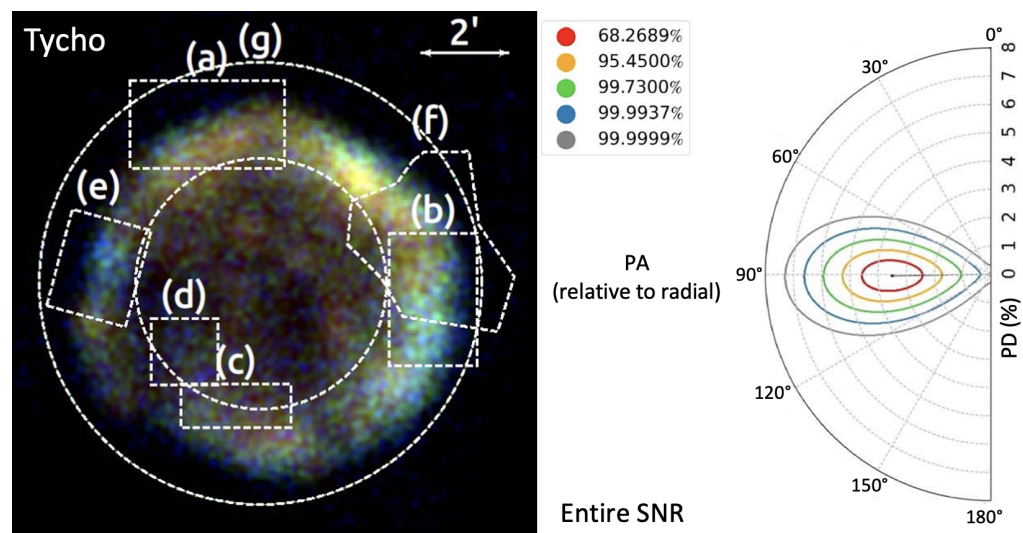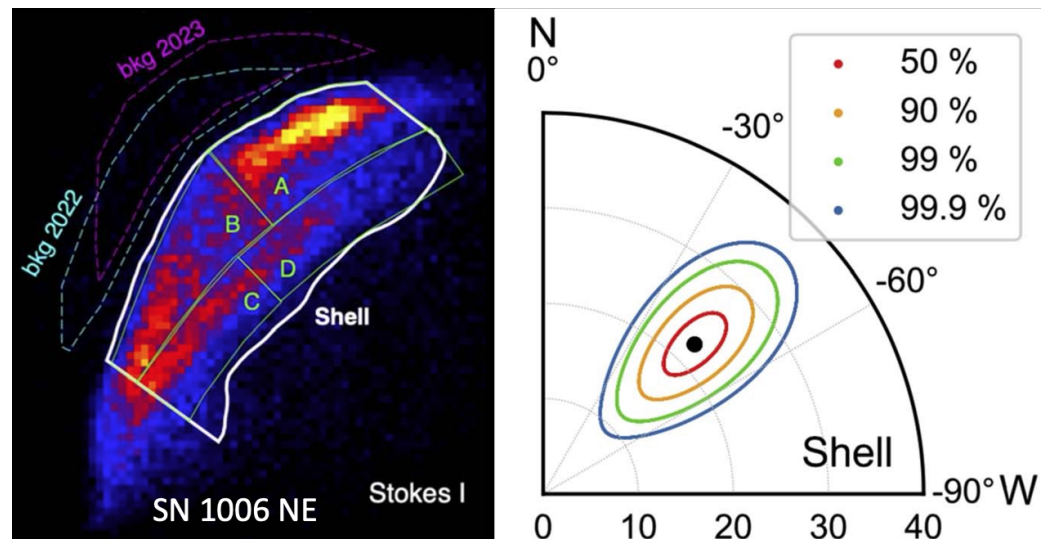

Figure 2. **Left**: IXPE image of Tycho. Labels identify specific regions investigated in [38]—the northeast knot (a); the western (b) and southern (c) nonthermal stripes and the nonthermal arc region (d); and regions in which strong polarization is detected (e,f). **Right**: Polar plot for entire SNR (region g). The polarization degree is indicated on the radial axis and the polarization angle is shown, with 0° corresponding to the radial direction; an angle of 90° indicates a radial magnetic field direction. The contours show significance levels.

4. SN 1006

SN 1006 is the first SNR detected to show strong nonthermal X-ray emission [39], making it a good target for X-ray polarimetry. The IXPE observed the northeastern shell of SN 1006 (SN 1006 NE) on 5–19 August 2022 and 3–10 March 2023, with a total effective exposure of ~960 ks [40]. Compared to Cas A and Tycho's SNR, that of SN 1006 is much fainter in X-rays. The background contributes a non-negligible fraction of the photons from the source region, and thus we removed this part in the analysis.

The IXPE resolved the double-rim structure of SN 1006 NE and allowed for a spatial analysis of the X-ray polarization. The IXPE Stokes I image of SN 1006 NE in 2–4 keV is shown in Figure 3, where the white and green polygon regions denote the shell region and four sub-scale regions, respectively. The X-ray polarization of the overall shell was detected at a significance of 6.3σ, with a polarization degree of $22.4 \pm 3.5\%$ and a polarization angle of $-45.5°$. The sub-scale regions A–C all show similar polarization properties with a significance between 3.4 and 4.6, while region D is marginally detected (2.5σ). These results suggest that the polarization degree does not significantly vary across the NE shell and magnetic fields are nearly radially distributed. We also used a different approach—spectropolarimetric analysis—to calculate the polarization of these five regions and obtained consistent results.

Figure 3. Left: IXPE image of the NE limb of SN 1006. Labels identify discrete portions of the shell investigated in [40]. **Right**: Polar plot for entire shell region. The polarization angle is shown with $0°$ corresponding to North. An angle of $\sim-45°$ corresponds to tangential polarization, and thus a radial magnetic field. The contours show significance levels.

SN 1006 has been measured in radio polarimetry [41]. Assuming a constant rotation measure, RM = 12 rad m^{-2}, we calculated the radio polarization results for SN 1006 NE and compared them with the IXPE values. We found a larger polarization angle of $-36.3° \pm 0.4°$ and a lower polarization degree of $14.5 \pm 0.2\%$ in the radio band. Since the radio results, especially the polarization angle, were influenced by the RM distribution, which was not well constrained in previous radio observations, we did not expand the discussion about the discrepancy between the two bands. However, a lower polarization degree in the radio band is not unexpected. First, the maximum polarization degree depends on the photon index, Γ: $PD_{max} = \Gamma/(\Gamma + 2/3)$. The X-ray spectrum is steeper than the radio band, suggesting a larger PD_{max}. Secondly, due to the shorter lifetime of the high-energy electrons, the synchrotron X-ray emission is from a thinner area than that of the radio emission, meaning that the radio emission is likely subject to stronger depolarization.

5. RX J1713.7−3946

RX J1713.7−3946 is a large (≈1 degree diameter) shell-type SNR residing in the Galactic plane, discovered by the ROSAT all-sky survey [42]. The remnant is at a distance of ∼1 kpc [43–45] and is thought to be the result of a Type Ib/c supernova explosion, possibly associated to the historical SN 393 [46–48], making it the oldest SNR whose results have been reported by the IXPE so far. Its hard X-ray emission is purely nonthermal [49,50], representing the second detection of synchrotron X-ray radiation from an SNR shell after SN 1006. Tsuji et al. [47] measured the shock velocity in the northwestern region to be ∼3900 km s^{-1}, with other structures within the NW shell, however, being significantly slower, down to ∼1400 km s^{-1}. Previous attempts at measuring radio polarization led to detections at the northwestern part of the shell, although Faraday rotation made it impossible to determine the magnetic field direction from the polarization vectors [51]. RX J1713.7−3946 is also one of the best studied young SNRs in the γ-ray band and one of the most debated sources in the discussion on the hadronic vs. leptonic origin of the high energy emission.

The IXPE observed the northwestern part of the shell of RX J1713.7−3946 three times in 2023, 24–27 August, 28 August to 1 September, and 24 September to 5 October, for a total exposure time of ∼841 ks [52].

In the left panel of Figure 4, the regions of interest selected for the analysis and the background extraction regions are shown. Significant polarization is found for all identified regions other than the broad western region (W). For the N and S regions, the polarization degree is modest (∼12–18%), while for the individual regions P1–P3, identified with high significance in binned maps, the values are as high as ∼45%. From both the polarization map and the regions of interest, our analysis found that the polarization direction is normal to the shock and that the average PD in the whole region is 13.0 ± 3.5%. Thus, whereas the other IXPE remnants all showed radial magnetic fields, RX J1713.7−3946 represents the first example for which shock-compressed tangential magnetic fields dominate in the X-ray band. These results are consistent with a model of shock compression of an upstream isotropic turbulence producing a predominantly tangential magnetic field.
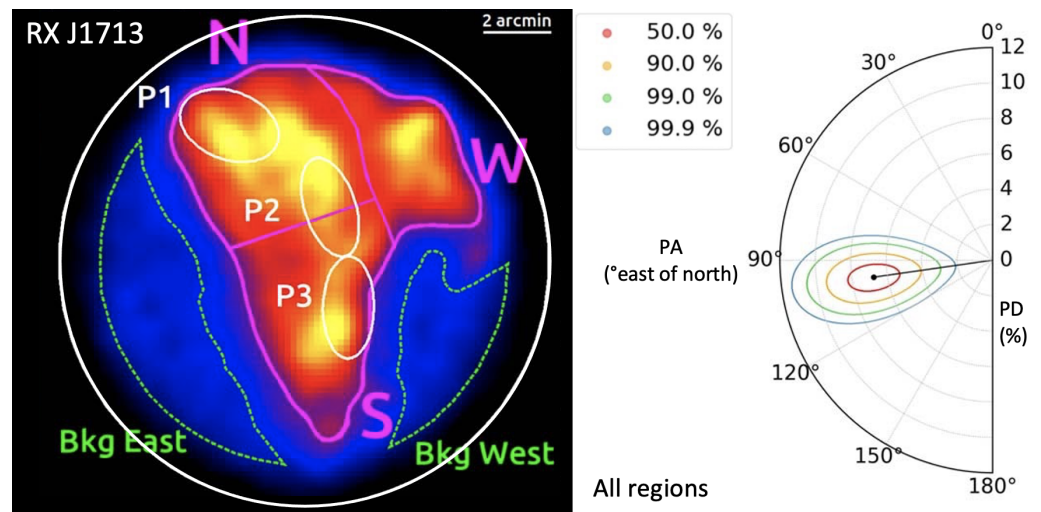
Figure 4. Left: IXPE image of the NW limb of RX J1713.7−3946. Labels identify north, west, and south (N, W, S) regions of the extended emission structure and discrete regions P1–P3 that show evidence for higher polarization—all were investigated in [52]. **Right**: Polar plot for entire limb region, composed of N + W + S. The polarization angle is measured from north to east, with an angle of ∼100° corresponding to the radial direction from the center of RX J1713.7−3946 and, thus, to a magnetic field that is tangential to the shock surface. The contours show significance levels.

6. Discussion

The polarization results from IXPE observations of young SNRs show that the polarization degree is quite small (Table 1), indicating high levels of turbulence in the immediate post-shock regions, as expected from models for diffusive shock acceleration with magnetic field amplification. It is noteworthy that the level of circumstellar medium (CSM) interaction—indicated by the ambient density, n_0—is high in Cas A (the product of a core-collapse SN expanding into a CSM highly modified by the progenitor star), modest in Tycho (but not zero; despite being the remnant of a Type Ia SN, Tycho shows evidence of CSM interactions), and small in SN 1006 (a Type Ia remnant located high above the Galactic plane). The polarization degree varies in the opposite sense, decreasing with increasing CSM interaction. It is conceivable that high levels of turbulence are associated with higher CSM densities, and that this results in a low polarization degree downstream. Models for the development of turbulent cascades predict different polarization properties for different levels of initial isotropy, with isotropic fields yielding small PD values [35], similar to those observed for Cas A [22].

Table 1. Polarization and physical parameters for IXPE SNRs.

	Polarization Degree (%) [a]			V_{shock} (km s^{-1})	n_0 (cm^{-3})	Bohm Factor (η)	B_{low}^{b} (μG)
	Rim	SNR	Peak				
Cas A	4.5 ± 1.0	2.5 ± 0.5	~15	~5800	0.9 ± 0.3	~1–6	25–40
Tycho	12 ± 2	9 ± 2	23 ± 4	~4600	~0.1–0.2	~1–5	30–40
SN 1006 (NE)	22.4 ± 3.5	...	31 ± 8	~5000	~0.05–0.08	~6–10	18–26
RX J1713 (W)	13.0 ± 3.5	...	46 ± 10	1400–2900	~0.01–0.2	~1.4	~10

(a) X-ray polarization degree for SNR rim, entire SNR, and peak value within SNR. (b) Lower limit to post-shock magnetic field based on rim width, e.g., [20].

Importantly, for Cas A, Tycho, and SN 1006, the measured polarization angle implies radial magnetic fields very close to the acceleration sites. Because particle acceleration in strong non-relativistic shocks is most efficient for parallel and quasi-parallel magnetic fields [53], this result may reflect a selection effect, with emission arising predominantly from regions where acceleration is efficient [7]. However, turbulence driven by rippled shocks resulting from encounters with upstream density fluctuations can result in dynamo-induced magnetic field amplification with the radial component dominating the downstream field, even for largely isotropic upstream turbulence [8]. Simulations [9] show that density fluctuations associated with the Bell instability [4] produced by streaming cosmic ray currents can produce such an effect, yielding predominately radial fields in the downstream region under conditions of high shock velocities and modest density.

For RX J1713.7−3946 the X-ray polarization results are quite different. While the polarization degree at the SNR rim is low, as for other SNRs for which the Bohm factor, η, approaches 1 (see Table 1), the inferred magnetic field direction is tangential instead of radial. This is typical of older SNRs in which the field in the post-shock region is dominated by the component compressed by the shock. For fast shocks with strong Bell instabilities, the radial magnetic field component can peak close to the shock and dominate the tangential component, while for slower shocks like those in RX J1713.7−3946, the radial field may peak further downstream, beyond the synchrotron cooling length of the X-ray-emitting electrons, thus resulting in a dominant tangential field [9].

IXPE studies of additional SNRs, with a range of ages and inferred Bohm factors, are underway to provide additional constraints on the connection between polarization properties and the remnant conditions. Measurements of the polarization degree and magnetic field geometry will continue to provide new insights into the conditions leading to efficient particle acceleration in fast shocks.

Conflicts of Interest: The authors declare no conflict of interest.

References

1. Malkov, M.A.; Drury, L. O'C Nonlinear theory of diffusive acceleration of particles by shock waves. *Rep. Prog. Phys.* **2001**, *64*, 429. [CrossRef]
2. Reynolds, S.P. Supernova remnants at high energy. *Annu. Rev. Astron. Astrophys.* **2008**, *46*, 89–126. [CrossRef]
3. Zirakashvili, V.N.; Aharonian, F. Analytical solutions for energy spectra of electrons accelerated by nonrelativistic shock-waves in shell type supernova remnants. *Astron. Astrophys.* **2007**, *465*, 695–702. [CrossRef]
4. Bell, A.R. Turbulent amplification of magnetic field and diffusive shock acceleration of cosmic rays. *Mon. Not. R. Astron. Soc.* **2004**, *353*, 550–558. [CrossRef]
5. Dickel, J.R.; Milne, D.K. Magnetic fields in supernova remnants. *Aust. J. Phys.* **1976**, *29*, 435–460. [CrossRef]
6. Dubner, G.; Giacani, E. Radio emission from supernova remnants. *Astron. Astrophys.* **2015**, *23*, 3–48. [CrossRef]
7. West, J.L.; Jaffe, T.; Ferrand, G.; Safi-Harb, S.; Gaensler, B.M. When Disorder Looks Like Order: A New Model to Explain Radial Magnetic Fields in Young Supernova Remnants. *Astrophys. J. Lett.* **2017**, *849*, L22. [CrossRef]
8. Inoue, T.; Shimoda, J.; Ohira, Y.; Yamazaki, R. The Origin of Radially Aligned Magnetic Fields in Young Supernova Remnants. *Astrophys. J. Lett.* **2013**, *772*, L20. [CrossRef]
9. Bykov, A.M.; Osipov, S.M.; Uvarov, Y.A.; Ellison, D.C.; Slane, P. X-ray polarization: A view deep inside cosmic ray driven turbulence and particle acceleration in supernova remnants. *Phys. Rev. D* **2024**, *110*, 023041. [CrossRef]
10. Reed, J.E.; Hester, J.J.; Fabian, A.C.; Winkler, P.F. The Three-dimensional Structure of the Cassiopeia A Supernova Remnant. I. The Spherical Shell. *Astrophys. J.* **1995**, *440*, 706. [CrossRef]
11. Vink, J.; Bloemen, H.; Kaastra, J.; Bleeker, J. The expansion of Cassiopeia A as seen in X-rays. *Astron. Astrophys.* **1998**, *339*, 201–207.
12. Patnaude, D.J.; Fesen, R.A. Proper Motions and Brightness Variations of Nonthermal X-ray Filaments in the Cassiopeia A Supernova Remnant. *Astrophys. J.* **2009**, *697*, 535. [CrossRef]
13. Anderson, M.C.; Keohane, J.W.; Rudnick, L. The Polarization and Depolarization of Radio Emission from Supernova Remnant Cassiopeia A. *Astrophys. J.* **1995**, *441*, 300. [CrossRef]
14. Rosenberg, I. Distribution of brightness and polarization in Cassiopeia A at 5.0 GHz. *Mon. Not. R. Astron. Soc.* **1970**, *151*, 109. [CrossRef]
15. Braun, R.; Gull, S.F.; Perley, R.A. Physical process which shapes Cassiopeia A. *Nature* **1987**, *327*, 395–398. [CrossRef]
16. Favata, F.; Vink, J.; dal Fiume, D.; Parmar, A.N.; Santangelo, A.; Mineo, T.; Preite-Martinez, A.; Kaastra, J.S.; Bleeker, J.A.M. The broad-band X-ray spectrum of the CAS A supernova remnant as seen by the BeppoSAX observatory. *Astron. Astrophys.* **1997**, *324*, L49–L52.
17. Allen, G.E.; Keohane, J.W.; Gotthelf, E.V.; Petre, R.; Jahoda, K.; Rothschild, R.E.; Lingenfelter, R.E.; Heindl, W.A.; Marsden, D.; Gruber, D.E.; et al. Evidence of X-ray Synchrotron Emission from Electrons Accelerated to 40 TeV in the Supernova Remnant Cassiopeia A. *Astrophys. J. Lett.* **1997**, *487*, L97–L100. [CrossRef]
18. Hughes, J.P.; Rakowski, C.E.; Burrows, D.N.; Slane, P.O. Nucleosynthesis and Mixing in Cassiopeia A. *Astrophys. J. Lett.* **2000**, *528*, L109–L113. [CrossRef]
19. Hwang, U.; Laming, J.M.; Badenes, C.; Berendse, F.; Blondin, J.; Cioffi, D.; DeLaney, T.; Dewey, D.; Fesen, R.; Flanagan, K.A.; et al. A Million Second Chandra View of Cassiopeia A. *Astrophys. J. Lett.* **2004**, *615*, L117. [CrossRef]
20. Vink, J.; Laming, J.M. On the Magnetic Fields and Particle Acceleration in Cassiopeia A. *Astrophys. J.* **2003**, *584*, 758–769. [CrossRef]
21. Bamba, A.; Yamazaki, R.; Yoshida, T.; Terasawa, T.; Koyama, K. A Spatial and Spectral Study of Nonthermal Filaments in Historical Supernova Remnants: Observational Results with Chandra. *Astrophys. J.* **2005**, *621*, 793. [CrossRef]
22. Vink, J.; Prokhorov, D.; Ferrazzoli, R.; Slane, P.; Zhou, P.; Asakura, K.; Baldini, L.; Bucciantini, N.; Costa, E.; Di Marco, A.; et al. X-ray Polarization Detection of Cassiopeia A with IXPE. *Astrophys. J.* **2022**, *938*, 40. [CrossRef]

23. Green, D.; Stephenson, F. Historical Supernovae. In *Supernovae Gamma-ray Bursters*; Springer: Berlin/Heidelberg, Germany, 2003; Volume 598, pp. 7–19.

24. Williams, B.; Coyle, N.; Yamaguchi, H.; Depasquale, J.; Seitenzahl, I.; Hewitt, J.; Blondin, J.; Borkowski, K.; Ghavamian, P.; Petre, R.; et al. The Three-dimensional Expansion of the Ejecta from Tycho's Supernova Remnant. *Astrophys. J.* **2017**, *842*, e28. [CrossRef]

25. Williams, B.; Katsuda, S.; Cumbee, R.; Petre, R.; Raymond, J.; Uchida, H. RGS Observations of Ejecta Knots in Tycho's Supernova Remnant. *Astrophys. J. Lett.* **2020**, *898*, eL51. [CrossRef]

26. Kundu, M.; Velusamy, T. Polarization of Tycho's Supernova Remnant at a Wavelength of 2.8 Centimeters. *Astrophys. J.* **1971**, *163*, 231. [CrossRef]

27. Strom, R.; Duin, R. A High Resolution 21 CM Continuum Study of the Supernova Remnants 3C 10 (Tycho's Supernova) and 3C 461 (Cas A). *Astron. Astrophys.* **1973**, *25*, 351–362.

28. Dickel, J.; Van Breugel, W.; Strom, R. Radio Structure of the Remnant of Tycho's Supernova (SN 1572). *Astron. J.* **1991**, *101*, 2151. [CrossRef]

29. Duin, R.; Strom, R. A multifrequency study of the radio structure of 3C 10, the remnant of Tycho's supernova. *Astron. Astrophys.* **1975**, *39*, 33–42.

30. Reynoso, E.; Moffett, D.; Goss, W.; Dubner, G.; Dickel, J.; Reynolds, S.; Giacani, E. A VLA Study of the Expansion of Tycho's Supernova Remnant. *Astrophys. J.* **1997**, *491*, 816–828. [CrossRef]

31. Hwang, U.; Decourchelle, A.; Holt, S.; Petre, R. Thermal and Nonthermal X-ray Emission from the Forward Shock in Tycho's Supernova Remnant. *Astrophys. J.* **2002**, *581*, 1101–1115. [CrossRef]

32. Eriksen, K.; Hughes, J.; Badenes, C.; Fesen, R.; Ghavamian, P.; Moffett, D.; Plucinsky, P.; Rakowski, C.; Reynoso, E.; Slane, P. Evidence for Particle Acceleration to the Knee of the Cosmic Ray Spectrum in Tycho's Supernova Remnant. *Astrophys. J. Lett.* **2011**, *728*, eL28. [CrossRef]

33. Okuno, T.; Tanaka, T.; Uchida, H.; Aharonian, F.; Uchiyama, Y.; Tsuru, T.; Matsuda, M. Time Variability of Nonthermal X-ray Stripes in Tycho's Supernova Remnant with Chandra. *Astrophys. J.* **2020**, *894*, e50. [CrossRef]

34. Matsuda, M.; Tanaka, T.; Uchida, H.; Amano, Y.; Tsuru, T. Temporal and spatial variation of synchrotron X-ray stripes in Tycho's supernova remnant. *Publ. Astron. Soc. Jpn.* **2020**, *72*, e85. [CrossRef]

35. Bykov, A.; Uvarov, Y.; Slane, P.; Ellison, D. Uncovering Magnetic Turbulence in Young Supernova Remnants with Polarized X-ray Imaging. *Astrophys. J.* **2020**, *899*, e142. [CrossRef]

36. Bykov, A.; Uvarov, Y.; Bloemen, J.; Den Herder, J.; Kaastra, J. A model of polarized X-ray emission from twinkling synchrotron supernova shells. *Mon. Not. R. Astron. Soc.* **2009**, *399*, 1119–1125. [CrossRef]

37. Bykov, A.; Ellison, D.; Osipov, S.; Pavlov, G.; Uvarov, Y. X-ray Stripes in Tycho's Supernova Remnant: Synchrotron Footprints of a Nonlinear Cosmic-ray-driven Instability. *Astrophys. J. Lett.* **2011**, *735*, eL40. [CrossRef]

38. Ferrazzoli, R.; Slane, P.; Prokhorov, D.; Zhou, P.; Vink, J.; Bucciantini, N.; Costa, E.; Di Lalla, N.; Di Marco, A.; Soffitta, P.; et al. X-ray Polarimetry Reveals the Magnetic-field Topology on Sub-parsec Scales in Tycho's Supernova Remnant. *Astrophys. J.* **2023**, *945*, e52. [CrossRef]

39. Koyama, K.; Petre, R.; Gotthelf, E.V.; Hwang, U.; Matsuura, M.; Ozaki, M.; Holt, S.S. Evidence for shock acceleration of high-energy electrons in the supernova remnant SN1006. *Nature* **1995**, *378*, 255–258. [CrossRef]

40. Zhou, P.; Prokhorov, D.; Ferrazzoli, R.; Yang, Y.-J.; Slane, P.; Vink, J.; Silvestri, S.; Bucciantini, N.; Reynoso, E.;Moffett, D.; et al. Magnetic Structures and Turbulence in SN 1006 Revealed with Imaging X-ray Polarimetry. *Astrophys. J.* **2023**, *957*, 55–69. [CrossRef]

41. Reynoso, E.M.; Hughes, J.P.; Moffett, D.A. On the Radio Polarization Signature of Efficient and Inefficient Particle Acceleration in Supernova Remnant SN 1006. *Astron. J.* **2013**, *145*, 104–112. [CrossRef]

42. Pfeffermann, E.; Aschenbach, B. ROSAT observation of a new supernova remnant in the constellation Scorpius. *Roentgenstrahlung Universe* **1996**, *2*, 267–268.

43. Fukui, Y.; Moriguchi, Y.; Tamura, K.; Yamamoto, H.; Tawara, Y.; Mizuno, N.; Onishi, T.; Mizuno, A.; Uchiyama, Y.; Hiraga, J.; et al. Discovery of Interacting Molecular Gas toward the TeV Gamma-ray Peak of the SNR G 347.3-0.5. *Publ. Astron. Soc. Jpn.* **2003**, *55*, L61–L64. [CrossRef]

44. Cassam-Chenaï, G.; Decourchelle, A.; Ballet, J.; Sauvageot, J.; Dubner, G.; Giacani, E. XMM-Newton observations of the supernova remnant RX J1713.7-3946 and its central source. *Astron. Astrophys.* **2004**, *427*, 199–216. [CrossRef]

45. Uchiyama, Y.; Aharonian, F.; Takahashi, T. Fine-structure in the nonthermal X-ray emission of SNR RX J1713.7-3946 revealed by Chandra. *Astron. Astrophys.* **2003**, *400*, 567–574. [CrossRef]

46. Wang, Z.; Qu, Q.; Chen, Y. Is RX J1713.7-3946 the remnant of the AD393 guest star? *Astron. Astrophys.* **1997**, *318*, L59–L61.

47. Tsuji, N.; Uchiyama, Y. Expansion measurements of supernova remnant RX J1713.7-3946. *Publ. Astron. Soc. Jpn.* **2016**, *68*, e108. [CrossRef]

48. Acero, F.; Katsuda, S.; Ballet, J.; Petre, R. Measurement of the X-ray proper motion in the south-east rim of RX J1713.7-3946. *Astron. Astrophys.* **2017**, *597*, eA106. [CrossRef]

49. Koyama, K.; Kinugasa, K.; Matsuzaki, K.; Nishiuchi, M.; Sugizaki, M.; Torii, K.; Yamauchi, S.; Aschenbach, B. Discovery of nonthermal X-rays from the Northwest Shell of the New SNR RX J1713.7-3946: The Second SN 1006? *Publ. Astron. Soc. Jpn.* **1997**, *49*, L7–L11. [CrossRef]

50. Slane, P.; Gaensler, B.; Dame, T.; Hughes, J.; Plucinsky, P.; Green, A. Nonthermal X-ray Emission from the Shell-Type Supernova Remnant G347.3-0.5. *Astrophys. J.* **1999**, *525*, 357–367. [CrossRef]

51. Lazendic, J.; Slane, P.; Gaensler, B.; Reynolds, S.; Plucinsky, P.; Hughes, J. A High-Resolution Study of Nonthermal Radio and X-ray Emission from Supernova Remnant G347.3-0.5. *Astrophys. J.* **2004**, *602*, 271–285. [CrossRef]

52. Ferrazzoli, R.; Prokhorov, D.; Bucciantini, N.; Slane, P.; Vink, J.; Cardillo, M.; Yang, Y.; Silvestri, S.; Zhou, P.; Costa, E.; et al. Discovery of a Shock-compressed Magnetic Field in the Northwestern Rim of the Young Supernova Remnant RX J1713.7-3946 with X-ray Polarimetry. *Astrophys. J. Lett.* **2024**, *967*, eL38. [CrossRef]

53. Caprioli, D.; Spitkovsky, A. Simulations of Ion Acceleration at Non-relativistic Shocks. I. Acceleration Efficiency. *Astrophys. J.* **2014**, *783*, 91. [CrossRef]